Mon. Not. R. Astron. Soc. **000**, 000–000 (0000) Printed 31 July 2014 (MN LATEX style file v2.2)

ALMA and *Herschel* Observations of the Prototype Dusty and Polluted White Dwarf G29-38

J. Farihi[1,2⋆†], M. C. Wyatt[2], J. S. Greaves[3], A. Bonsor[4,5], B. Sibthorpe[6], O. Panić[2]
[1]*Department of Physics and Astronomy, University College London, London WC1E 6BT*
[2]*Institute of Astronomy, University of Cambridge, Cambridge CB3 0HA*
[3]*School of Physics and Astronomy, University of St Andrews, St Andrews KY16 9SS*
[4]*School of Physics, University of Bristol, Bristol BS8 1TL*
[5]*Institute de Planétiology, Universityé Joseph Fourier, BP 53, 38041, Grenoble Cedex 9, France*
[6]*SRON Netherlands Institute for Space Research, P.O. Box 800, 9700 AV Groningen, The Netherlands*

arXiv:1407.7976v1 [astro-ph.EP] 30 Jul 2014

ABSTRACT

ALMA Cycle 0 and *Herschel*[1] PACS observations are reported for the prototype, nearest, and brightest example of a dusty and polluted white dwarf, G29-38. These long wavelength programs attempted to detect an outlying, parent population of bodies at $1 - 100$ AU, from which originates the disrupted planetesimal debris that is observed within 0.01 AU and which exhibits $L_{\rm IR}/L_* = 0.039$. No associated emission sources were detected in any of the data down to $L_{\rm IR}/L_* \sim 10^{-4}$, generally ruling out cold dust masses greater than $10^{24} - 10^{25}$ g for reasonable grain sizes and properties in orbital regions corresponding to evolved versions of both asteroid and Kuiper belt analogs. Overall, these null detections are consistent with models of long-term collisional evolution in planetesimal disks, and the source regions for the disrupted parent bodies at stars like G29-38 may only be salient in exceptional circumstances, such as a recent instability. A larger sample of polluted white dwarfs, targeted with the full ALMA array, has the potential to unambiguously identify the parent source(s) of their planetary debris.

Key words: circumstellar matter— stars: abundances— stars: individual (G29-38)— planetary systems— white dwarfs

1 INTRODUCTION

1.1 Discovery and Characterization of G29-38

More than a quarter century has passed since the discovery of infrared excess emission from the nearby white dwarf G29-38 (Zuckerman & Becklin 1987). Photometric observations conducted at the NASA Infrared Telescope Facility atop Mauna Kea in the K, L, and M bands revealed flux in excess of that expected for the relatively cool white dwarf. While a warm dust disk was considered a possibility, the infrared excess was initially attributed to a spatially unresolved brown dwarf. In particular, 1000 K circumstellar dust was considered unlikely due to rapid dissipation from radiation drag. Prophetically, Zuckerman & Becklin (1987) noted that if material were orbiting sufficiently close to achieve such a high temperature, then spectral signatures of accretion should be seen.

Within a few years, and thanks to intense observational and theoretical interest from a diverse set of researchers, evidence began to disfavor a substellar companion as the origin of the infrared emission. First, some of the earliest infrared imaging arrays revealed G29-38 to be a point source in all available bandpasses. Second, near-infrared spectroscopy measured a thermal continuum (Tokunaga et al. 1988), whereas a very cool atmosphere was expected to exhibit absorption features. Third, the detection of optical stellar pulsations echoed in the near-infrared were difficult to reconcile with a brown dwarf secondary (Patterson et al. 1991; Graham et al. 1990). Fourth and finally, significant 10 μm emission was detected at G29-38, at a level a few times greater than expected for an object with a Jupiter-sized radius, essentially ruling out the brown dwarf companion hypothesis (Tokunaga et al. 1990; Telesco et al. 1990).

A decade after the discovery of its infrared excess, the optical and ultraviolet spectroscopic detection of multiple metal species in the atmosphere of G29-38 (Koester et al.

⋆ E-mail: j.farihi@ucl.ac.uk
† STFC Ernest Rutherford Fellow
[1] *Herschel* is an ESA space observatory with science instruments provided by European-led Principal Investigator consortia and with important participation from NASA.

© 0000 RAS

1997) made it clear that the star was accreting from its immediate environs. Although white dwarfs with metal absorption features have been known for nearly a century (vMa 2; van Maanen 1917), the source of the heavy elements had never been observationally identified and the closely orbiting disk at G29-38 was the smoking gun.

1.2 Tidally-Destroyed Planetesimals

In a seminal paper, Jura (2003) modeled the observed properties of G29-38 by invoking a tidally-destroyed minor planet (i.e. large asteroid) that evolves into an opaque, flat ring of dust analogous to the rings of Saturn. The particles are heated by the star, producing an infrared excess, and slowly dragged down onto the stellar surface, polluting its otherwise-pristine atmosphere with heavy elements. The tidally-disrupted asteroid model has seen continued success since its inception, and is considered the standard model for metal-enriched white dwarfs. In the intervening decade, an enormous amount of observational progress has occurred (for a detailed review, see Farihi 2011), all of which supports the accretion of asteroid-like debris in dynamically active, post-main sequence planetary systems (Veras et al. 2013).

1. Over 30 metal-lined white dwarfs are now known to exhibit $T \sim 1000\,\mathrm{K}$ thermal emission from disks (e.g. Xu & Jura 2012; Brinkworth et al. 2012; Girven et al. 2012; Farihi et al. 2012, 2010b, 2009; Jura et al. 2007; von Hippel et al. 2007; Kilic et al. 2006); their properties are precisely as expected for material contained within the Roche limit of the star and feeding the stellar surface (Metzger et al. 2012; Rafikov 2011; Bochkarev & Rafikov 2011). A fraction of these exhibit metallic, gaseous emission (Farihi et al. 2012; Melis et al. 2012, 2011; Gänsicke et al. 2008, 2007, 2006) that is spatially coincident with the particulate disks (Brinkworth et al. 2012; Melis et al. 2010).

2. All dusty white dwarfs observed with IRS on *Spitzer* exhibit strong silicate emission features consistent with olivines, (Jura et al. 2009a; Reach et al. 2009; Lisse et al. 2008; Reach et al. 2005), and which are also seen in the infrared spectra of evolved solids associated with planet formation (Lisse et al. 2008).

3. The elemental abundances in disk-polluted white dwarfs are universally depleted in volatile elements (especially carbon and hydrogen), and have a refractory rich pattern that broadly mimics the terrestrial material of the inner Solar System (Jura & Young 2014; Gänsicke et al. 2012; Klein et al. 2010; Zuckerman et al. 2007). All data acquired to date are consistent with rocky parent bodies that formed interior to a snow line (Farihi et al. 2013; Jura & Xu 2012), including evidence for differentiation (Jura et al. 2013; Gänsicke et al. 2012; Zuckerman et al. 2011; Farihi et al. 2011).

4. The collective properties of all published ($N \sim 250$ as of this writing), metal-polluted white dwarfs support the accretion of planetary debris for the population at large (Zuckerman et al. 2010; Farihi et al. 2010a; Zuckerman et al. 2003), including even those stars that do not exhibit detectable infrared excesses (Rocchetto et al. 2014). These findings imply that at least 30% (Koester et al. 2014) of cool white dwarfs have the signatures of large planetesimals, whose size estimated diameters range from ~ 10 to $\sim 1000\,\mathrm{km}$ (Wyatt et al. 2014; Jura & Young 2014).

Table 1. Multi-wavelength Fluxes and Upper Limits for G29-38

Source	$\lambda_{\rm eff}$ (μm)	F_ν (mJy)
GALEX	0.15	3.4
GALEX	0.23	10.9
U	0.37	17.3
B	0.44	21.7
V	0.55	22.3
R	0.64	18.8
I	0.80	15.1
J	1.24	8.9
H	1.66	6.0
K_s	2.16	5.6
IRAC	3.55	8.4
IRAC	4.49	8.8
IRAC	5.73	8.4
IRAC	7.87	8.4
IRTF	10.5	11.1
IRS	16.0	3.7
MIPS	23.7	2.4
MIPS	71.4	< 1.3
PACS	100	< 1.6
PACS	160	< 4.4
ALMA	870	< 0.17
ALMA	1305	< 0.21

Note. Fluxes are *GALEX* far- and near-ultraviolet (Martin et al. 2005), ground-based $UBVRIJHK_sN$ (Landolt & Uomoto 2007; Skrutskie et al. 2006; Tokunaga et al. 1990), *Spitzer* IRAC, IRS 16 and MIPS 24 μm photometry (Farihi et al. 2008; Reach et al. 2005). Also listed are 3σ upper limits from MIPS 70 μm photometry (Jura et al. 2009b), and the similar PACS and ALMA limits reported here.

1.3 Motivation for Long Wavelength Data

All successful models for disks at white dwarfs invoke tidally-destroyed planetary bodies that originate in a more distant and substantially more massive reservoir of planetesimals (Frewen & Hansen 2014; Debes et al. 2012; Bonsor et al. 2011; Jura 2003; Debes & Sigurdsson 2002). To date, there have been no indications of cooler dust associated with an outlying planetesimal population around metal-polluted white dwarfs, but the longest wavelength observations conducted for a substantial number of stars are both *WISE* 22 μm and *Spitzer* MIPS 24 μm photometry (Hoard et al. 2013; Farihi et al. 2009; Jura et al. 2007). These data only probe for dust at radii of 1 to a few AU for typical $10\,000 - 20\,000\,\mathrm{K}$ white dwarfs, and thus longer wavelength data are needed to search for populations analogous to the asteroid and Kuiper belts of the Solar System.

This paper presents *Herschel* (Pilbratt et al. 2010) far-infrared and ALMA submillimeter observations of G29-38 (ZZ Psc, WD 2326+049). This iconic stellar remnant has a hydrogen-dominated atmosphere of $T_{\rm eff} \approx 12\,000\,\mathrm{K}$, intrinsic brightness $\log(L/L_*) \approx -2.5$, and a cooling age near 380 Myr (Giammichele et al. 2012; Fontaine et al. 2001).

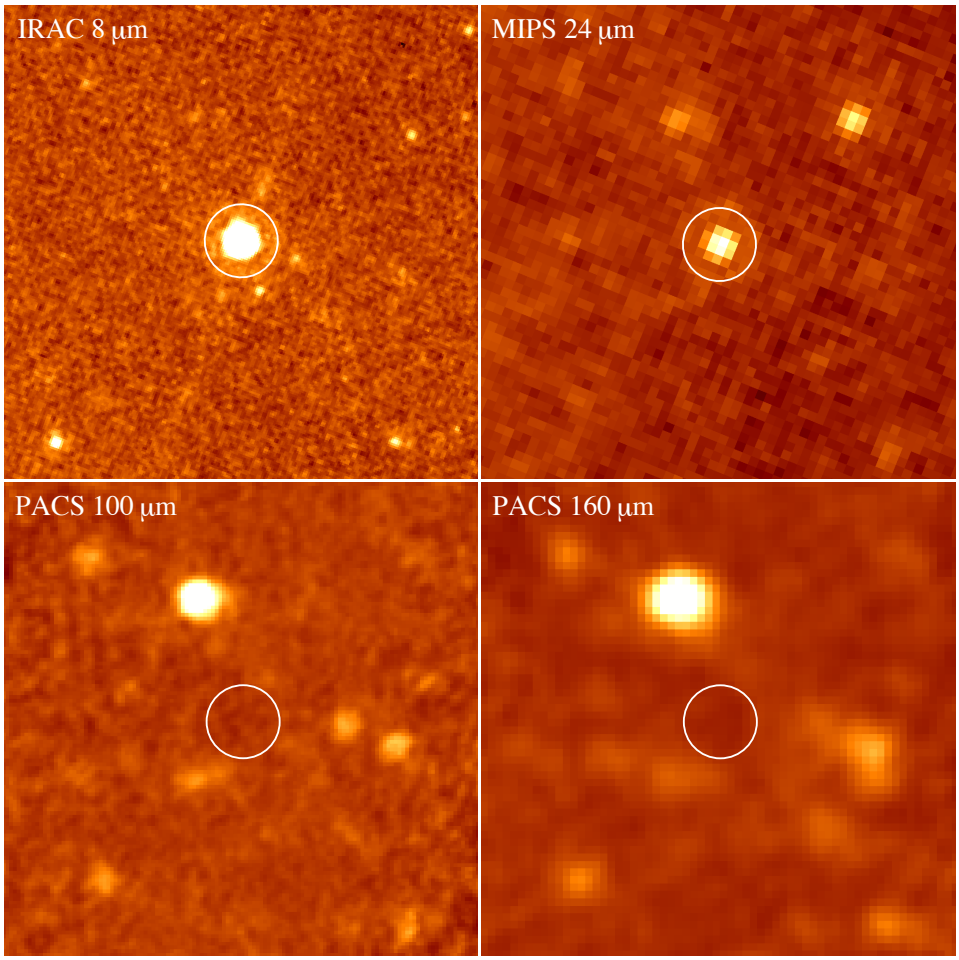

Figure 1. Reduced infrared images of G29-38 taken with both *Spitzer* and *Herschel*. The images are north up and east left and approximately 125″ on a side. Accounting for its proper motion of $0\farcs49\,\mathrm{yr}^{-1}$, the expected location of G29-38 is marked by a circle in each image, with emission only detected in the *Spitzer* data.

At 13.6 pc, G29-38 is the nearest example of a disk-polluted white dwarf and also the brightest by an order of magnitude, making it ideal for long wavelength observations sensitive to cold dust emission, and where a ring of $20-200$ AU diameter would span $1\farcs4-14''$ on the sky and be potentially resolved.

Both sets of observations resulted in null detections, and provide limits on cold dust masses similar to known Kuiper belt objects. The observations and data analysis details are presented in §2, from which are derived sensitivities to fractional dust luminosity, and similarly to dust masses, as a function of temperature and orbital radius for all existing $\lambda \geqslant 70\,\mu$m observations. The results are presented in §3 together with a comparison of these data and sensitivities with known dusty A-type stars, which represent possible progenitors of the G29-38 system.

2 OBSERVATIONS AND DATA

2.1 *Herschel*

G29-38 was targeted by the *Herschel Space Observatory* on 2012 June 6 with the Photodetector Array Camera and Spectrometer (PACS; Poglitsch et al. 2010) at 100 and 160 μm. These data are particularly sensitive to 20 K dust in the 10 AU region, where any emission at these wavelengths is expected to be unresolved at the $7''/100\,\mu$m diffraction limit of a 3.5 m telescope. While circumstellar dust orbiting beyond $50-80$ AU can be spatially resolved around nearby stars with *Herschel* (e.g. Booth et al. 2013), the very low luminosity of a cool white dwarf like G29-38 makes such a detection unlikely (see §3.1).

The source was expected to be substantially fainter than the 50 mJy limit recommended for standard chop-nod observations, and thus the mini-scan map mode was used. These were executed in three pairs of cross-scans, using individual cross-scan angles of 70°and 110°, and each of the six segments repeated 25 times for an on-source time of 1800 s. In total, G29-38 was observed for 3.0 hr on source and with 9.4 hr observatory time.

The PACS data were reduced using the *Herschel* Interactive Processing Environment (HIPE) version 7.0. The data were processed using the standard PACS photometer processing steps, and maps were made using the PHOTPROJECT task. The data were high-pass filtered in the scan direction with filter width of 66″ and 102″ (equivalent to 16 and 25 frames) in the 100 and 160 μm bands respectively. The fully reduced images are shown in Figure 1 alongside *Spitzer* imaging detections in the mid-infrared.

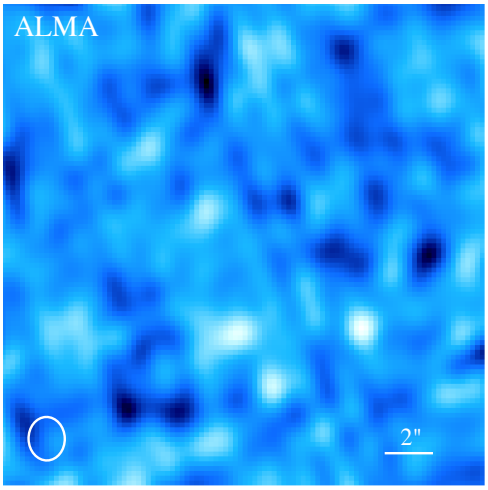

Figure 2. Bands 6 and 7, beam-combined ALMA image centered on the expected position of G29-38. The image is north up and east left, with the band 7 beam size and orientation shown in the lower left, and the spatial scale given in the lower right. No sources are detected above $3\sigma \approx 0.17$ mJy.

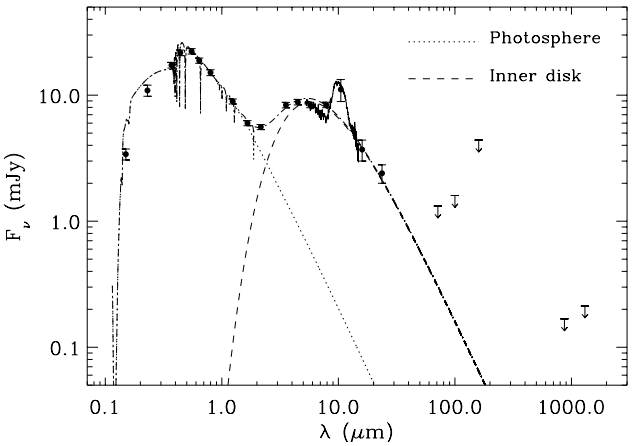

Figure 3. Extended spectral energy distribution of G29-38. Details of the measured fluxes and 3σ upper limits are listed in Table 1 and discussed in §2. The dotted line is a stellar atmosphere model, the dashed line is a face-on, flat and optically thick ring model ($T_{\rm in} = 1250$ K, $T_{\rm in} = 650$ K) fitted to the warm disk continuum emission, and the solid line the measured strong silicate feature in the *Spitzer* IRS SL spectrum (Reach et al. 2009).

The source was assumed to be point-like and photometry was performed using apertures. Source apertures with radii of 5″ and 8″ (0.7×FWHM, which is near optimal for a point source) were used for the 100 and 160 μm bands respectively. The field background and 1σ noise were obtained by taking the median and standard deviation of multiple apertures, with radii equal to that of the source apertures, located within 1′ of the source location respectively. The measured fluxes ($F_{100,160\mu{\rm m}} = -0.5, -0.6$ mJy), and sum in noise apertures ($\sigma_{100,160\mu{\rm m}} = 0.7, 1.6$ mJy), have all had aperture corrections applied; 1.94 and 1.90 for the 100 and 160 μm bands respectively. The derived upper limits for G29-38 are the flux measured in the source apertures $+3\sigma$, and are listed in Table 1.

2.2 ALMA

G29-38 was also observed with the Atacama Large Millimeter/Submillimeter Array (ALMA) as part of Early Science operations at the beginning of Cycle 0 in 2011 November. Data were acquired over the course of several nights, with two 17 min observations on 18 and 26 November in band 6 (230 GHz, 1305 μm), and five 23 minutes observations on 6, 14, and 16 November in band 7 (345 GHz, 870 μm). During the brief time span of the observations, the proper motion of G29-38 was negligible for the concatenation of datasets. All but two observations were made using 15 antennas, but a single observation in each of band 6 and 7 was made with 17 and 14 antennas respectively. The spatial configuration of the array provided baselines covering a range from 10 to 150 m.

Initial calibrations and pointing were done on the bright quasars 3C 454.3 and 3C 446, while Neptune was used for absolute flux calibration. The science observations were interleaved with the phase calibrator J2323−032. The observing setup was the most sensitive for continuum observations, using the wide-band TDM mode with 128 15625 MHz wide spectral channels, 2 MHz bandwidth per polarization, and resulting in a full effective bandwidth of 7.5 MHz.

The data were processed by the ALMA pipeline and the achieved RMS values were 0.071 mJy/beam in band 6 and 0.056 mJy/beam in band 7; these were adopted as the 1σ noise values. No sources were detected in either band, and upper limits for unresolved emission from the science target were taken to be 3σ and are listed in Table 1. Using the Common Astronomy Software Applications package, a band 6 and 7, beam-combined image was created to increase the chance of source detection using the increased signal and spectral information. No emission from the science target is evident in these merged down to $3\sigma \approx 0.17$ mJy. The beam-combined image is displayed in Figure 2, and is overplotted with the band 7 beam size (1.″5×1.″8 at position angle 1.63°).

3 ANALYSIS AND DISCUSSION

3.1 Sensitivity to Dust Emission

Figure 3 details the spectral energy distribution of G29-38, extending from the ultraviolet to submillimeter wavelengths. The stellar photosphere is detected from the far-ultraviolet until the near-infrared, where the spatially unresolved emission of the inner disk dominates at $\lambda > 2\,\mu$m. Of the suite of available data, the ALMA observations had the best ability to spatially resolve any emission from dust, but only for relatively cold and distant material beyond 11 AU.

Following Wyatt (2008), all the available infrared and submillimeter upper limit F_ν at G29-38 were transformed into limiting fractional disk luminosities as a function of dust temperature and corresponding orbital radius using

$$f = 3.4 \times 10^9 F_\nu d^2 X_\lambda / r^2 B_\nu(\lambda, T) \quad (1)$$

where d is the distance to the star, r the orbital radius of dust grains of temperature T, and B_ν is the Planck function.

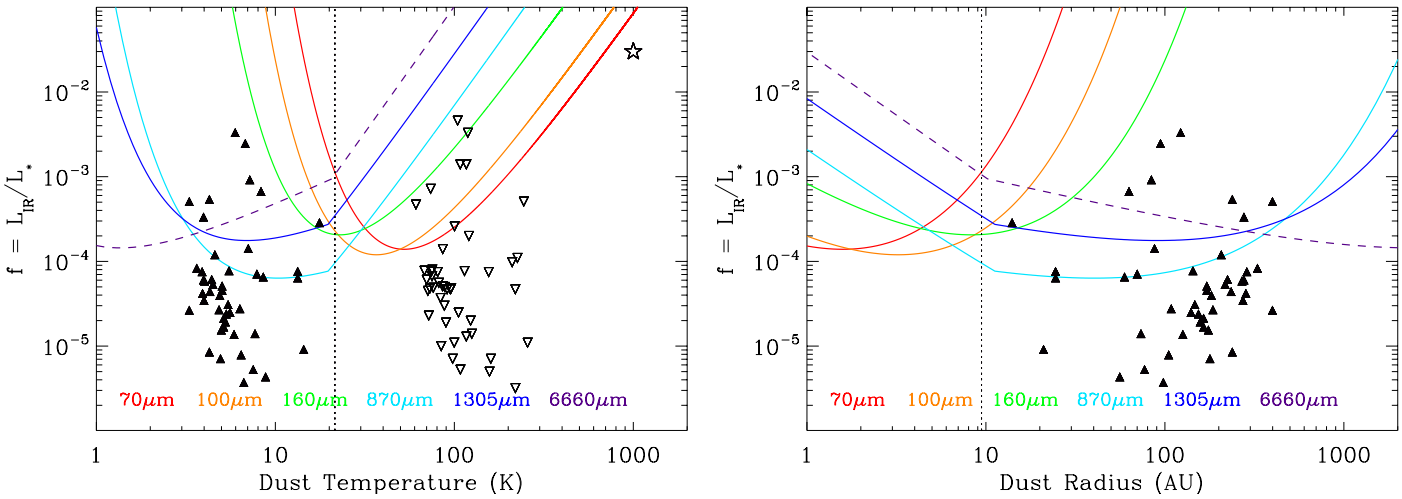

Figure 4. Upper limit sensitivity curves for all long wavelength non-detections of G29-38 as a function of dust fractional luminosity, temperature, and orbital radius; only the area above each curve was detectable in individual observations. Limits with *Spitzer* MIPS 70 μm are shown in red, *Herschel* PACS 100 and 160 μm in orange and green respectively, and ALMA 870 and 1305 μm in light and dark blue respectively. The ALMA sensitivities have been corrected for spatially-resolved emission from dust beyond 11.2 AU (below roughly 20 K for blackbody grains). Also shown as a dashed purple line are predictions for the EVLA at 45 GHz in the most favorable configuration (§3.1). The filled triangles are evolved, cool white dwarf stage projections (§3.2) of known, dusty A-type stars (Su et al. 2006), while the progenitor systems are shown as open, inverted triangles in the left panel. The observations as a whole were particularly sensitive to evolved main belt analogs, shown as a dotted line in each plot. The star symbol in the upper right corner of the left-hand panel is the (undetected) known warm disk, orbiting interior to 0.01 AU.

The factor X_λ allows for the faster falloff in emission towards longer wavelengths for non-blackbody – smaller, warmer yet more distant– grains (Williams & Andrews 2006). These upper limit fractional dust luminosities are plotted as colored curves in Figure 4 for the *Spitzer*, *Herschel*, and ALMA observations. Also included in the plot is a similar curve for the most compact configuration of the Expanded Very Large Array (EVLA) at 45 GHz, with a 1.″5 beam, and a 5.6 μJy continuum sensitivity (Perley et al. 2011).

Any blackbody dust grains with temperature below approximately 20 K would be orbiting beyond 11 AU and hence be spatially resolved to some degree in the ALMA observations, which had a band 7 beam diameter between 1.″5 and 1.″8, and thus capable of resolving ring structures with radii larger than $10.2 - 12.2$ AU at 13.6 pc (see Figure 2). The plotted ALMA sensitivities were corrected for such resolved cases by assuming a face on disk and dividing by the number of beams per ring circumference. The sensitivities of the *Herschel* observations were similarly corrected for dust located beyond $50 - 80$ AU, but it is worth noting that such high fractional luminosities 1) lie above the Figure 4 plots and cannot be assumed to be optically thin, and 2) would have been detected as spatially resolved emission with ALMA.

3.2 Projections of Dusty A-type Stars

Also in Figure 4 are plotted model extrapolations for dusty A-type stars from Su et al. (2006), as their *current* dust properties would appear if the host stars were evolved into cool white dwarfs with parameters similar to G29-38. To begin, the inferred orbital radii of the dust components on the main sequence were expanded by a factor $r_{\rm wd}/r_{\rm ms} = M_{\rm ms}/M_{\rm wd} \approx 3.5$, appropriate for G29-38 and a representative value for A stars based on the initial-to-final mass relations (e.g. Williams et al. 2009; Kalirai et al. 2008). This change not only leads to a change in dust grain temperatures, but also in their illumination. The amount of light intercepted by the dust decreases by $(r_{\rm ms}/r_{\rm wd})^2$, but the total emitting area of the dust *increases* because small grains are not removed by radiation pressure (Farihi et al. 2008). On the main sequence the collisional cascade is truncated at a grain diameter that is approximately $L_{\rm ms}/M_{\rm ms}$ (Artymowicz 1988), and thus the emitting area and fractional luminosity is proportional to $1/\sqrt{L_{\rm ms}/M_{\rm ms}}$.

Following Bonsor & Wyatt (2010), considering the realistic emission properties of small grains illuminated by the faint white dwarf, only particles larger than 0.1 μm contribute significantly to the emission, and thus the change in fractional luminosity will be

$$f_{\rm wd}/f_{\rm ms} \approx (r_{\rm ms}/r_{\rm wd})^2 \times \left(\sqrt{L_{\rm ms}/M_{\rm ms}}/\sqrt{0.1}\right) \quad (2)$$

Notably, several of the brightest A-star debris disk projections were readily detectable in the ALMA (but not *Herschel* or *Spitzer*) observations, even with the modest number of antennae and corresponding limited sensitivity. However, it is important to note that these modeled points: 1) are based on disks orbiting relatively young, main sequence stars, 2) essentially preserve the mass of colliding planetesimals between stellar phases, and 3) allow arbitrarily cold dust, including temperatures below that supported by ambient interstellar radiation. A fixed minimum temperature for dust grains that is substantially warmer than the 3 K cosmic microwave background will favorably impact their detectability with ALMA as such a disk will tend towards the more sensitive parts of the Figure 4 curves, while the assumption of no further collisional evolution nor dust depletion (e.g. wind

drag or dynamical) over the course of stellar evolution, are admittedly physically unrealistic.

While small dust grains would be removed during the asymptotic giant phase, they are quickly replenished by collisions. The collision rate of the largest surviving particles can be long, but the smallest grains are repopulated from the integrated collisions of all large bodies, resulting in a replenishment timescale equal to their depletion timescale in a steady state (Wyatt et al. 2011). Still, detailed models for the post-main sequence evolution of Kuiper belt analogs (Bonsor et al. 2011; Bonsor & Wyatt 2010) suggest that detecting these disks in cool white dwarf systems like G29-38 is challenging, primarily due to collisional depletion of the disc material. Such collisional depletion would occur on even shorter timescales for asteroid belt analogs favored by the volatile poor abundance patterns seen via atmospheric pollution (Gänsicke et al. 2012; Jura & Xu 2012), including G29-38 in particular (Xu et al. 2014). And while searches for cold disks have been carried out with *Spitzer* in more favorable, hot (pre-)white dwarf systems with relatively high stellar luminosity (Chu et al. 2011; Su et al. 2007), the resulting picture is complicated by binarity and dusty outflows associated with their immediate progenitors (Clayton et al. 2014).

The stochastic planetesimal accretion models of Wyatt et al. (2014) place G29-38 among the top 1% of accretors in terms of incoming material, but it is also notable among DA stars where instantaneous rates can be inferred from observed metal abundances. If white dwarf pollution were correlated with disk brightness on the main sequence, then G29-38 would have evolved from one of the brightest main sequence disks and thus imply the highest chance of cold dust detection among polluted white dwarfs. The fact that it is not detected, and the fact that the young dusty A star disks are predicted to be detectable in the absence of depletion of their belts, may support, but not strongly, the likelihood that such main sequence disks, on average, become depleted in dust as they progress significantly beyond their current, relatively young ages.

These caveats notwithstanding, the analysis and figures indicate that in the absence of significant depletion, or in the case of where debris is replenished in these orbital regions (e.g. Stone et al. 2014), that ALMA is an excellent tool to both detect and spatially resolve disks at white dwarfs. Giant impacts or instabilities analogous to the late heavy bombardment would substantially increase the detectability of planetesimal disks at white dwarfs, and cold dust can accumulate over long timescales due to the feeble stellar luminosity. Another possibility that favors the retention of substantial disk mass is if the planetesimals have high eccentricity and thus a reduced collision rate (Wyatt et al. 2010). While the average planetesimal disk at white dwarfs may be depleted, some fraction of the population may remain salient. The final ALMA array of 66 dishes should more than double the sensitivity, all else being equal, and thus be capable of detecting circumstellar dust more representative of current A stars, as well as asteroid belt analogs, now cold and expanded beyond several AU.

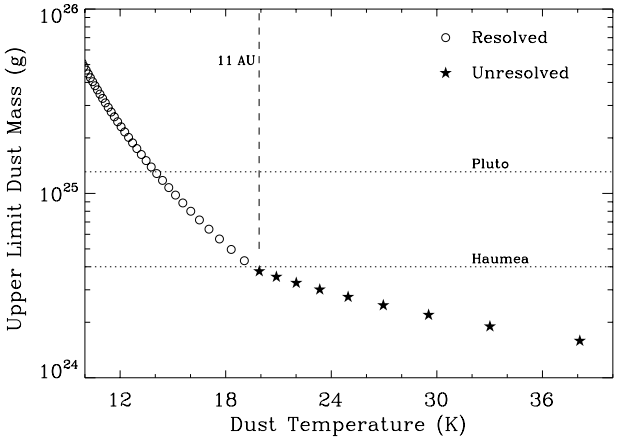

Figure 5. Dust mass limits calculated from the achieved ALMA upper limit at 870 μm of 0.17 mJy. For dust warmer than around 20 K the emission is expected to remain spatially unresolved in the observations, while cooler dust would have been spread across many beams and thus the sensitivity drops accordingly.

3.3 Dust Mass Limits

To derive upper limits on the mass of dust present around G29-38, the 870 μm observations were the most sensitive for realistic temperatures. Emission at this wavelength traces predominantly millimeter sized dust particles and is most likely optically thin. In the absence of any detailed information on the composition and size of any grains associated with this source, the average value of dust opacity is adopted here, $\kappa = 1.7\,\mathrm{cm^2\,g^{-1}}$ at 870 μm, noting that the actual opacity may be anywhere in the range $0.2 - 4.0\,\mathrm{cm^2\,g^{-1}}$ (Draine 2006).

Using a radial dependence of the dust temperature identical to that derived in §3.1 and plotted in Figure 4, the adopted upper limit flux of $F_\nu = 0.17$ mJy/beam is converted to the dust mass using

$$m(T) = F_\nu d^2 / \kappa B_\nu(T) \quad (3)$$

A range of radial distances r were explored, where dust emission falls within one half of the primary beam of a 12 m ALMA antenna at 870 μm, or up to 60 AU from the star. Having no information on the radial or azimuthal distribution of dust, nor its projected distance in the plane of the sky, the calculations assume a simple, circular, and face-on ring of radial thickness much less than the beam size (22 AU at 13.6 pc).

Spatially unresolved emission allows direct conversion from the observed flux to the mass of the dust using the above expression, while at $2r > 22$ AU the ring would become resolved and the observed flux per beam is then a fraction of the total flux in the ring. Upper limits derived in this way are shown in Figure 5, where only high dust masses greater than that of Pluto (1.3×10^{25} g) can be ruled out beyond 11 AU in the spatially resolved regime. In the case of unresolved emission within 11 AU, the upper limit dust masses are relatively low and comparable to a few times the mass of Ceres (9.4×10^{23} g).

Coincidentally, the unresolved dust mass limits fall within a factor of a few of the highest known masses of metals residing in the outer layers of polluted white dwarfs

with significant convection zones (Dufour et al. 2010; Farihi et al. 2010a). However, there is no reason to expect a physical connection between collisionally generated dust masses in outer planetesimal belts (which requires replenishment over appropriate timescales), and the amount of mass that is transported via (presumably) intact parent bodies to the tidal disruption radius, and later the stellar surface, of polluted white dwarfs.

4 OUTLOOK

Debris from the inferred parent population of planetesimals at G29-38 remains undetected with *Herschel* PACS at 100 and 160μm, and ALMA in early and relatively shallow observations at 870 and 1305 μm. While the ALMA observations were best suited to outer regions analogous to evolved Kuiper belt analogs, the *Herschel* data were uniquely sensitive to an evolved, asteroid-like belt at G29-38 and in general to dust at temperatures and orbital regions intermediate to the relatively warm dust seen at polluted white dwarfs and the cooler dust often detected at main sequence stars. The non-detection at G29-38 is not wholly unexpected, as disk evolution models supported by observations of main sequence stars predict that the available mass in both dust and parent bodies decreases significantly over timescales of several hundred Myr (Wyatt et al. 2007), and this depletion is likely enhanced during the post-main sequence (Bonsor & Wyatt 2010).

These data collectively preclude a relatively bright, $L_{\rm IR}/L_* > 10^{-4}$ disk in the general vicinity of 10 AU around the nearest and brightest polluted white dwarf with an infrared excess. From orbital expansion alone, a planetesimal belt currently in within 10 AU would have orbited within the terrestrial zone – interior to the water ice line – during the main sequence, and thus be consistent with the suspected source regions for parent bodies of the disk of disrupted and polluting material in G29-38 and a growing number of white dwarfs where detailed abundance measurements allow a robust assessment of their volatile content (Koester et al. 2014; Xu et al. 2014; Farihi et al. 2013; Gänsicke et al. 2012; Jura & Xu 2012). Therefore, any dusty asteroid-like belt must lie below these detection limits.

However, recent work suggests that it is difficult for sufficient material to survive to the white dwarf phase in this inner region (Frewen & Hansen 2014; Debes et al. 2012). A parent body origin in an outer, Kuiper-like belt remains consistent with these long wavelength observations (Bonsor et al. 2011), but the volatile deficiency combined with substantial parent body masses, both inferred via atmospheric pollution remains to be explained.

While significant uncertainty remains, ALMA is the only current facility able to empirically constrain the source regions for the parent bodies of the planetary debris surrounding and falling onto white dwarfs like G29-38.

ACKNOWLEDGMENTS

The authors are grateful to Anita Richards and the UK ARC at the University of Manchester for observation and data analysis support, and to the anonymous reviewer for suggestions that improved the manuscript. This paper makes use of the following ALMA data: ADS/JAO.ALMA #2011.0.00851.S (PI Farihi). ALMA is a partnership of ESO (representing its member states), NSF (USA), and NINS (Japan), together with NRC (Canada), NSC and ASIAA (Taiwan), in cooperation with the Republic of Chile. The Joint ALMA Observatory is operated by ESO, AUI/NRAO and NAOJ. *Herschel* is an ESA space observatory with science instruments provided by European-led Principal Investigator consortia and with important participation from NASA. J. Farihi gratefully acknowledges the support of the STFC via an Ernest Rutherford Fellowship. A. Bonsor acknowledges the support of the ANR-2010 BLAN-0505-01 (EXOZODI). M. C. Wyatt and O. Panić are grateful for the support of the European Union through ERC grant number 279973.

REFERENCES

Artymowicz P. 1988, ApJ, 335, L79
Bochkarev K. V., Rafikov R. R. 2011, ApJ, 741, 36
Bonsor A., Wyatt M. 2010, MNRAS, 409, 1631
Bonsor A., Mustill A. J., Wyatt M. 2011, MNRAS, 414, 930
Booth M., et al. 2013, MNRAS, 428, 1263
Brinkworth C. S., Gänsicke B. T., Girven J., Hoard D. W., Marsh T. R., Parsons S. G., Koester D. 2012, ApJ, 750, 86
Chu Y. H., et al. 2011, AJ, 142, 75
Clayton G. C., De Marco O., Nordhaus J., Green J., Rauch T., Werner K., Chu Y. H. 2014, AJ, 147, 142
Debes J. H., Sigurdsson S. 2002, ApJ, 572, 556
Debes J., Walsh K., Stark C. 2012, ApJ, 747, 148
Draine B. T. 2006, ApJ, 636, 1114
Dufour P., Kilic M., Fontaine G., Bergeron P., Lachapelle F. R., Kleinman S. J., Leggett S. K. 2010, ApJ, 719, 803
Farihi J. 2011, in White Dwarf Atmospheres and Circumstellar Environments, ed. D. W. Hoard (Berlin: Wiley-VCH), ISBN 978-3-527-41031-6
Farihi J., Brinkworth C. S., Gänsicke B. T., Marsh T. R., Girven J., Hoard D. W., Klein B., Koester D. 2011, ApJ, 728, L8
Farihi J., Barstow M. A., Redfield S., Dufour P., Hambly N. C. 2010a, MNRAS, 404, 2123
Farihi J., Gänsicke B. T., Steele P. R., Girven J., Burleigh M. R., Breedt E., Koester D. 2012, MNRAS, 421, 1635
Farihi J., Gänsicke B. T., Koester D. 2013, Science, 342, 218
Farihi J., Jura M., Lee J. E., Zuckerman B. 2010b, ApJ, 714, 1386
Farihi J., Jura M., Zuckerman B. 2009, ApJ, 694, 805
Farihi J., Zuckerman B., Becklin E. E. 2008, ApJ, 674, 431
Fontaine G., Brassard P., Bergeron P. 2001, PASP, 113, 409
Frewen S. F. N., Hansen B. M. S. 2014, MNRAS, 439, 2442
Gammie C. F., Menou K. 1998, ApJ, 492, L75
Gänsicke B. T., Koester D., Marsh T. R., Rebassa-Mansergas A., Southworth J. 2008, MNRAS, 391, L103
Gänsicke B. T., Koester D., Farihi J., Girven J., Parsons S. G., Breedt E. 2012, MNRAS, in press

Gänsicke B. T., Marsh T. R., Southworth J. 2007, MNRAS, 380, L35
Gänsicke B. T., Marsh T. R., Southworth J., Rebassa-Mansergas A. 2006, Science, 314, 1908
Giammichele N., Bergeron P., Dufour P. 2012, ApJS, 199, 29
Gianninas A., Bergeron P., Ruiz M. T. 2011, ApJ, 743, 2011
Girven J., Brinkworth C. S., Farihi J., Gänsicke B. T., Hoard D. W., Marsh T. R., Koester D. 2012, ApJ, 749, 154
Graham J. R., Matthews K., Neugebauer G., Soifer B. T. 1990, ApJ, 357, 216
Hoard D. W., Debes J. H., et al. 2013, ApJ, in press
Holberg J. B., Bergeron P. 2006, AJ,132, 1221
Jura M. 2003, ApJ, 584, L91
Jura M. 2008, ApJ,135, 1785
Jura M., Farihi J., Zuckerman B. 2007, ApJ, 663, 1285
Jura M., Farihi J., Zuckerman B. 2009a, AJ, 137, 3191
Jura M., Muno M. P., Farihi J., Zuckerman B. 2009b, ApJ, 699 1473
Jura M., Xu S. 2012, AJ, 143, 6
Jura M., Xu S., Young E. D. 2013, ApJ, 775, L41
Jura M., Xu S., Young E. D. 2014, AREPS, 42, 45
Kalirai J. S., Hansen B. M. S., Kelson D. D., Reitzel D. B., Rich R. M., Richer H. B. 2008, ApJ, 676, 594
Kilic M., von Hippel T., Leggett S. K., Winget D. E. 2006, ApJ, 646, 474
Klein B., Jura M., Koester D., Zuckerman B., Melis C. 2010, ApJ, 709, 950
Klein B., Jura M., Koester D., Zuckerman B. 2010, ApJ, 741, 64
Koester D., Gänsicke B. T., Farihi J. 2014, A&A, in press
Koester D., Provencal J., Shipman H. L. 1997, A&A, 230, L57
Landolt A. U., Uomoto A. K. 2007, AJ, 133, 768
Lisse C. M., Chen C. H., Wyatt, M. C., Morlok, A. 2008, ApJ, 673, 1106
Martin D. C., et al. 2005, ApJ, 619, L1
Melis C., Jura M., Albert L., Klein B., Zuckerman B. 2010, ApJ, 722, 1078
Melis C., Farihi J., Dufuour P., Zuckerman B., Burgasser A. J., Bergeron P., Bochanski J., Simcoe R. 2011, ApJ, 732, 90
Melis C., Dufour P., Farihi J., Bochanski J., Burgasser A. J., Parsons S. G., Gänsicke B. T., Koester D., Swift B. J. 2012, ApJ, 751, L4
Metzger B. D., Rafikov R. R., Bochkarev K. V. 2012, MNRAS, 423, 505
Patterson J., Zuckerman B., Becklin E. E., Tholen D. J., Hawarden T. 1991, ApJ, 374, 330
Perley R. A., Chandler C. J., Butler B. J., Wrobel J. M. 2011, ApJ, 739, L1
Pilbratt G.L., et al. 2010, A&A, 518, L1
Poglitsch A., et al. 2010, A&A, 518, L2
Rafikov R. R. 2011a, ApJ, 732, L3
Reach W. T., Kuchner M. J., von Hippel T., Burrows A., Mulally F., Kilic M., Winget D. E. 2005, ApJ, 635, L161
Reach W. T., Lisse C., von Hippel T., Mullally F. 2009, ApJ, 693, 697
Rocchetto M., Farihi J., Gänsicke B. T., Bergfors C. 2014, MNRAS, submitted
Skrutskie M. F., et al. 2006, AJ, 131, 1163
Stone N., Metzger B., Loeb A. 2014, MNRAS, in press (arXiv:1404.3213)
Su K. Y. L., et al. 2006, ApJ, 653, 675
Su K. Y. L., et al. 2007, ApJ, 657, L41
Telesco C. M., Joy M., Sisk C. 1990, ApJ, 358, L21
Tokunaga A. T., Becklin E. E., Zuckerman B. 1990, ApJ, 358, L17
Tokunaga A. T., Hodapp K. W., Becklin E. E., Cruikshank D. P., Rigler M., Toomey D. W., Brown R. H., Zuckerman B. 1988, ApJ, 332, L71
van Maanen A. 1917, PASP, 29, 258
Veras D., Mustill A., Bonsor A., Wyatt M. C. 2013, MNRAS, 431, 1686
von Hippel T., Kuchner M. J., Kilic M., Mullally F., Reach W. T. 2007, ApJ, 662, 544
Williams J. P. Andrews S. M. 2006, ApJ, 653, 1480
Williams K. A., Bolte M., Koester D. 2009, ApJ, 693, 355
Wyatt M. C. 2008, ARA&A, 46, 339
Wyatt M. C., Booth M., Payne M. J., Churcher L. J. 2010, MNRAS, 402, 657
Wyatt M. C., Clarke C. J., Booth M. 2011, CeMDA, 111, 1
Wyatt M. C., Farihi J., Pringle J. E., Bonsor A. 2014, MNRAS, 439, 3371
Wyatt M. C., Smith R., Greaves J. S., Beichman C. A., Bryden G., Lisse, C. M. 2007, ApJ, 658, 569
Xu S., Jura M. 2012, ApJ, 745, 88
Xu S., Jura M., Koester D., Klein B., Zuckerman B. 2014, ApJ, 783, 79
Zuckerman B., Becklin E. E. 1987, Nature, 330, 138
Zuckerman B., Koester D., Reid I. N., Hünsch M. 2003, ApJ, 596, 477
Zuckerman B., Koester D., Melis C., Hansen B. M. S., Jura M. 2007, ApJ, 671, 872
Zuckerman B., Melis C., Klein B., Koester D., Jura M. 2010, ApJ, 722, 725
Zuckerman B., Koester D., Dufour, P., Melis C., Klein B., Jura M. 2011, ApJ, 7239, 101